# Simulation Study of the Lithium Ion Transport Mechanism in Ternary Polymer Electrolytes: The Critical Role of the Segmental Mobility

Diddo Diddens*,[†] and Andreas Heuer

Institut für physikalische Chemie, Westfälische Wilhelms-Universität Münster, Corrensstrasse 28/30, 48149 Münster, Germany

Ⓢ *Supporting Information*

ABSTRACT: We present an extensive molecular dynamics (MD) simulation study of the lithium ion transport in ternary polymer electrolytes consisting of poly(ethylene oxide) (PEO), lithium-bis(trifluoromethane)sulfonimide (LiTFSI), and the ionic liquid *N*-methyl-*N*-propylpyrrolidinium bis(trifluoromethane)-sulfonimide (PYR$_{13}$TFSI). In particular, we focus on two different strategies by which the ternary electrolytes can be devised, namely by (a) *adding* the ionic liquid to PEO$_{20}$LiTFSI and (b) *substituting* the PEO chains in PEO$_{20}$LiTFSI by the ionic liquid. To grasp the changes of the overall lithium transport mechanism, we employ an analytical, Rouse-based cation transport model (Maitra et al. *Phys. Rev. Lett.* **2007**, *98*, 227802), which has originally been devised for binary PEO-based electrolytes. This

model distinguishes three different microscopic transport mechanisms, each quantified by an individual time scale. In the course of our analysis, we extend this mathematical description to account for an entirely new transport mechanism, namely, the TFSI-supported diffusion of lithium ions decoupled from the PEO chains, which emerges for certain stoichiometries. We find that the segmental mobility plays a decisive role in PEO-based polymer electrolytes. That is, whereas the addition of the ionic liquid to PEO$_{20}$LiTFSI plasticizes the polymer network and thus also increases the lithium diffusion, the amount of free, mobile ether oxygens reduces when substituting the PEO chains by the ionic liquid, which compensates the plasticizing effect. In total, our observations allow us to formulate some general principles about the lithium ion transport mechanism in ternary polymer electrolytes. Moreover, our insights also shed light on recent experimental observations (Joost et al. *Electrochim. Acta* **2012**, *86*, 330).
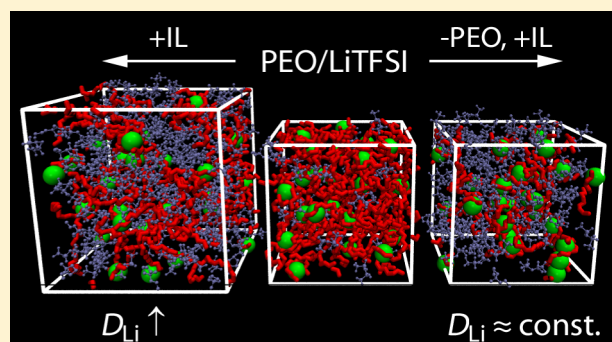
1. INTRODUCTION

Polymer electrolytes—typically consisting of an amorphous polymer matrix and a salt dissolved in it[1]—are promising candidates for many technological devices such as batteries or fuel cells.[2−4] Here, a commonly used polymer is poly(ethylene oxide) (PEO), whereas lithium-bis(trifluoromethane)-sulfonimide (LiTFSI) is often employed as a conducting salt, as the large TFSI anion reduces ion aggregation (see chemical structures in Figure 1). However, at ambient temperatures, the conductivity is still too low for an efficient technological use.

Several attempts have been made in the past to overcome this deficiency. Common modifications of the classical polymer−salt systems are the addition of nanoparticles[5] or organic solvent molecules.[6−8] However, in the case of the latter, the resulting electrolytes suffer from the high volatility and thus flammability of the solvent as well as from its reaction with lithium metal electrodes.[8] Here, Passerini et al.[9−12] demonstrated that the use of an ionic liquid (IL) instead of a conventional solvent has several advantages: The ILs are nonvolatile, nonflammable,[13] and exhibit a wide electrochemical stability window.[14−16] In this way, improved polymer electrolytes can be designed, which show an increased
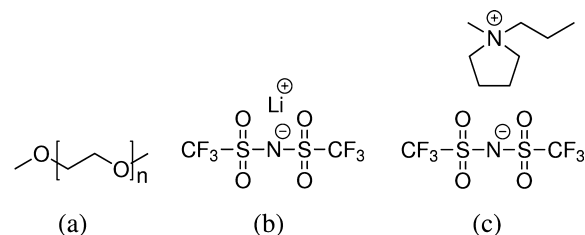

Figure 1. Chemical compounds simulated in this study: (a) poly(ethylene oxide) (PEO), (b) lithium-bis(trifluoromethane)-sulfonimide (LiTFSI), and (c) *N*-methyl-*N*-propylpyrrolidinium bis(trifluoromethane)sulfonimide (PYR$_{13}$TFSI).

conductivity combined with inherent stability,[9,12] and are thus ideal to create light-weight but powerful batteries.[10,11]

In a recent molecular dynamics (MD) simulation study,[17] we investigated a ternary polymer electrolyte consisting of PEO$_{20}$LiTFSI and a variable mole fraction *x* of the IL *N*-methyl-*N*-propylpyrrolidinium bis(trifluoromethane)-
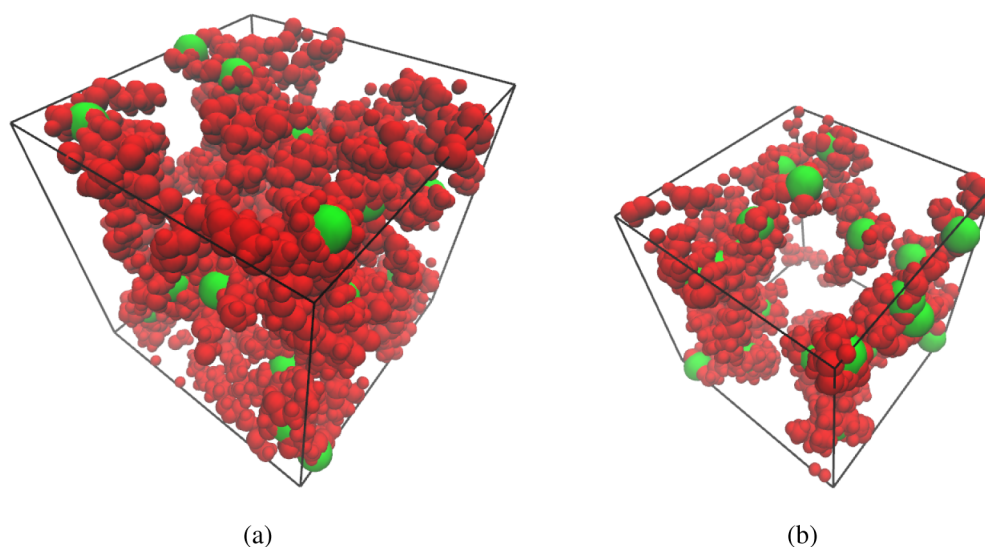
(a) (b)

Figure 2. Snapshots from the simulation showing (a) the *addition* of IL to the binary polymer electrolyte $PEO_{20}LiTFSI$ and (b) the *substitution* of PEO chains by IL molecules from the same electrolyte. PEO chains are shown in red and lithium ions in green, whereas all other ions (PYR_{13}^+ and $TFSI^-$) are invisible.

sulfonimide ($PYR_{13}TFSI$, see Figure 1). As observed experimentally by Passerini et al.,[9,12] we also found a clear increase of the lithium diffusion coefficient with x and were able to show that the main reason for this enhancement can be attributed to the plasticization of the PEO backbone by the IL. That is, the presence of the IL enhances the PEO dynamics, and consequently, the lithium ions coordinated to the PEO backbone also become faster.

In this contribution, we will significantly expand the scope of our previous analysis[17] and investigate the lithium transport in ternary polymer electrolytes in a more general way. This not only is due to the fact that we present additional insights on the ternary $PEO_{20}LiTFSI \cdot xPYR_{13}TFSI$ mixtures (in which IL is *added* to binary $PEO_{20}LiTFSI$) but also follow a conceptually different approach how to create ternary polymer electrolytes; that is, we also *substitute* PEO chains in $PEO_{20}LiTFSI$ by $PYR_{13}TFSI$ molecules. This procedure is carried out in such a way that the overall lithium volume concentration is held constant. Figure 2 shows snapshots from the simulations for the two different scenarios. The motivation for our extended study is 2-fold: First, although Passerini et al. found in their recent work[12] that the lithium diffusion coefficient increases with the IL fraction for an ether oxygen-to-lithium ion (EO:Li) ratio of 20:1, they simultaneously observed no significant changes for lower ratios of 10:1 or 5:1. This observation becomes even more puzzling by additional insights from Raman measurements,[12] which revealed that with increasing x the lithium–TFSI coordination increases at the expense of the lithium–PEO coordination (especially for low EO:Li ratios). Although these findings rather suggest a lithium transport mechanism which is at least partly decoupled from the PEO chains, it is obvious from the approximately constant lithium diffusion coefficients that the lithium motion cannot be similar to that in pure IL/LiTFSI electrolytes, which would be significantly faster.[18,19] Nevertheless, the transport mechanism has to change at some point when PEO is successively replaced by $PYR_{13}TFSI$ molecules, which gives us a second, theoretical motivation for our extended study. Thus, the concentration series of the PEO substitution serves as a model electrolyte in a double sense, as both the EO:Li ratio decreases with increasing

IL fraction and at the same time a crossover from a PEO-based lithium transport mechanism to a TFSI-based transport mechanism is enforced.

In addition to the MD simulations, we also employ an analytical ion transport model[20] to clarify the issues outlined above. This model expresses the macroscopic lithium diffusion in PEO-based polymer electrolytes via three different microscopic mechanisms, each characterized by a specific time scale (see sketch in Figure 3): (1) Diffusion along the PEO chain,
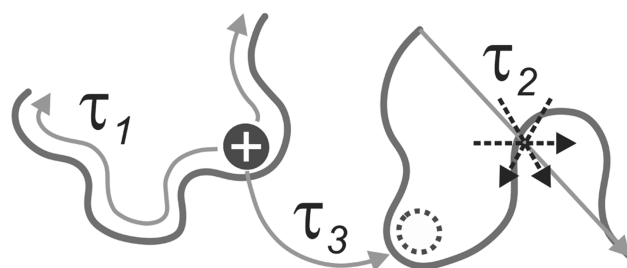

Figure 3. Sketch depicting the three different cation transport mechanisms in PEO–salt electrolytes. Each mechanism is characterized by a specific time scale.

which can be interpreted as an effective one-dimensional random walk along the curvilinear path of the polymer chain. This motion can be characterized by the time scale τ_1 the ion needs to explore the entire PEO chain. (2) Segmental motion of the PEO chain, which can be separated into the center-of-mass motion and the internal dynamics. For nonentangled chains, the internal dynamics can be described by the Rouse model[21] via an effective Rouse time τ_2, characterizing the motion of the bound PEO segments. (3) Intersegmental transfer of the cation from one PEO chain to another, which can be quantified by the average residence time τ_3 at a given chain. Previous simulations[20] have shown that this mechanism can be viewed as a renewal process within the framework of the dynamic bond percolation (DBP) model[22] since the dynamics of a given lithium ion becomes independent of its past after being transferred to another PEO chain. One particular

advantage of our model is that it allows one to extrapolate the lithium diffusion coefficients derived from the numerical data to the experimentally relevant long-chain limit.

However, one should keep in mind that the ion transport model has originally been developed for the archetypal, binary polymer electrolytes. Although our previous study[17] showed that the lithium transport mechanism qualitatively remains the same for the case of IL addition, it is a priori unclear if this also holds for the PEO substitution, as the transport mechanism will certainly change at some point when PEO is removed from the electrolyte. In fact, it will turn out that the IL-mediated lithium transport may substantially contribute to the overall lithium migration, and we will propose a revised model accounting for this additional, fourth transport mechanism.

Further advancements compared to our original study[17] are comprehensive analyses related to the microscopic factors contributing to the individual transport mechanisms. For example, we will demonstrate that the plasticization by the IL is only one important requirement to yield an enhanced segmental mobility and thus a faster lithium diffusion. Moreover, the effect of the IL on the polymer dynamics is also interesting from a fundamental point of view, as it gives rise to hydrodynamic interactions among distinct PEO segments, reflected by a Zimm-like scaling of the Rouse-mode relaxation times. Concerning the other mechanisms, we will show that, e.g., the renewal process (characterized by τ_3) can be understood in terms of a few structural and dynamical observables. These additional insights could ultimately contribute to a more directed improvement of battery materials.

For all ternary electrolytes, $PEO_{20}LiTFSI$ will be used as a reference. In what follows, the electrolytes with a constant EO:Li ratio, i.e., 20:1, and a variable amount x of $PYR_{13}TFSI$ will be denoted as $PEO_{20}LiTFSI \cdot xPYR_{13}TFSI$. The new electrolyte types, devised to study the differences in the lithium transport mechanisms between binary PEO/LiTFSI and $PYR_{13}TFSI/LiTFSI$, will be denoted as $PEO_{20-\alpha x}LiTFSI \cdot xPYR_{13}TFSI$. Here, α is the ratio of the respective partial molar volumes of a $PYR_{13}TFSI$ ion pair and a PEO monomer (see below).

For reasons of simplicity, we also abbreviate PEO as 'P' (i.e., polymer or PEO) and LiTFSI as 'S' (i.e., salt) in the following, leading to the short-hand notations $P_{20}S \cdot x$ IL and $P_{20-\alpha x}S \cdot x$ IL for the two distinct classes of ternary electrolytes.

This article is organized as follows: Section 2 describes the details of the MD simulation procedure and the setup of the systems. In Section 3, we discuss the lithium ion coordination sphere and the structure of the PEO chains. Section 4 deals with the two transport processes involving changes in the lithium coordination sphere (intersegmental transfer and diffusion along the chain), followed by a detailed analysis of the polymer dynamics (Section 5). Having characterized all three transport mechanisms, we compare the predictions of our model with the experimental data from Passerini et al.[12] (Section 6). Finally, we conclude (Section 7).

2. MD SIMULATION METHODOLOGY

The MD simulations were performed with a modified version of the sander module of the AMBER package,[23] allowing us to use a force field specifically designed for PEO/LiTFSI[24,25] and $PYR_{13}TFSI$[26] (see Supporting Information (SI), Section S2, for a validation of the modified AMBER code and Section S3 for a benchmark assessing its performance).

The initial configurations were created by randomly placing the individual molecules on a simple cubic lattice with a lattice constant of 36 Å irrespective of their type, mixing the system in this way. In the case of PEO, the chains already had coiled conformations as under melt conditions, thereby circumventing an expensive equilibration.

The binary PEO/LiTFSI electrolyte contained 10 PEO chains with $N = 54$ monomers each as well as 27 LiTFSI molecules. In the case of the addition of IL, i.e., $P_{20}S \cdot x$ IL, the simulation cell also contained 18 ($x = 0.66$) or 87 ($x = 3.24$) $PYR_{13}TFSI$ molecules. The latter system is shown in Figure 2(a). In the case of the substitution of PEO ($P_{20-\alpha x}S \cdot x$ IL) and thus a constant lithium volume concentration, the partial molar volumes of PEO and $PYR_{13}TFSI$ must be known. Through several short equilibration runs of the respective binary electrolytes, namely, $PEO_nLiTFSI$ ($n = 30, 20,$ and 10) and $PYR_{13}TFSI \cdot xLiTFSI$ ($x = 0.20, 0.24,$ and 0.26) in the NpT ensemble, we found that the molar volumes of both PEO and $PYR_{13}TFSI$ are independent of the LiTFSI fraction for the investigated concentration ranges. Their ratio reveals that approximately $\alpha = 7.14$ PEO monomers occupy the same volume as one $PYR_{13}TFSI$ ion pair. On the basis of this value, we created the following systems: 8 PEO chains with 15 $PYR_{13}TFSI$ molecules ($P_{16}S \cdot 0.556$ IL), 6 PEO chains with 30 $PYR_{13}TFSI$ molecules ($P_{12}S \cdot 1.111$ IL), and 4 PEO chains with 45 $PYR_{13}TFSI$ molecules ($P_8S \cdot 1.667$ IL, see Figure 2(b)), all of them containing, as above, 27 LiTFSI ion pairs. Neat PEO (16 chains with $N = 54$) and the pure $PYR_{13}TFSI/LiTFSI$ electrolyte (76 $PYR_{13}TFSI$ molecules and 27 LiTFSI ion pairs, $PYR_{13}TFSI \cdot 0.262$ LiTFSI) serve as a reference within this context.

The systems were equilibrated in the NpT ensemble for 70–80 ns using the PME technique.[27] Afterward, production runs with a total length of 200 ns were performed in the NVT ensemble. A time step of 1 fs was used in all simulations to propagate the systems. The temperature was maintained by the Berendsen thermostat[28] with a reference temperature of 423 K. All bonds involving hydrogen were constrained by the SHAKE algorithm.[29] The induceable point dipoles were integrated by a Car–Parrinello-like scheme,[30] and the charge–dipole interactions between atoms separated by three bonds (1–4 interactions) were scaled by a factor of 0.2. For all other nonbonded contributions, the full 1–4 interaction was taken into account. Dipole–dipole interactions were damped using a Thole screening[31] with a dimensionless damping parameter[24] of $a_T = 0.4$.

Table S1 (SI) shows the average values of the box lengths as determined from the NpT runs and subsequently used in the NVT simulations. One indeed observes that the box length is nearly the same for all $P_{20-\alpha x}S \cdot x$ IL systems. Slight deviations for $PYR_{13}TFSI \cdot 0.262$ LiTFSI may result from rounded molecule numbers in the simulation.

3. STRUCTURAL PROPERTIES

3.1. Lithium Coordination. To quantify the local structure around the lithium ions, radial distribution functions (denoted as $g(r)$ in the following) have been computed for the atom pairs Li^+-O_{PEO} and Li^+-O_{TFSI} (see Section S1.2, SI). Both coordination types exhibit a sharp peak around 2 Å, corresponding to the first coordination shell, which is in good agreement with neutron diffraction experiments[32] and quantum chemistry calculations.[33,34] At larger distances no significant structural arrangement can be found. When

successively adding the IL, one observes that the peak positions of both Li^+-O_{PEO} and Li^+-O_{TFSI} remain the same for all electrolytes. Thus, the same criterion to define temporary lithium bonds will be used for the subsequent analysis. We consider an EO and a Li^+ as bound if their distance is not larger than 3.0 Å. In analogy, we consider a Li^+ and a TFSI oxygen as bound if their distance is not larger than 2.7 Å.

The probability distribution functions to find a lithium ion with a certain number of EOs or TFSI oxygens in its first coordination shell is also shown in the SI (Figure S2). To summarize, we find that the predominant lithium coordination consists of 4−5 EOs for all electrolytes, which is again in good agreement with the experimental data[32] and the quantum-chemical results.[33,34] In those complexes where the 4−5 EOs originate from a single PEO molecule, the polymer chain wraps helically around the cation. For complexes involving two PEO chains, typically 2−3 EOs from each chain coordinate to the ion.

Coordinations by TFSI oxygens are mostly rare, and often the anion coordinates only briefly to the lithium ion (cf. Figure 2, where all ions are in the vicinity of a PEO chain). The only exceptions are $P_8S\cdot1.667$ IL and, though less pronounced, $P_{12}S\cdot1.111$ IL. Here, the lithium ions more likely coordinate to 1−2 TFSI oxygens in contrast to all other systems, and some are even coordinated to TFSI only (0.4% for $P_{12}S\cdot1.111$ IL and 2.5% for $P_8S\cdot1.667$ IL). As in pure IL/LiTFSI, the prevalent coordination number in the latter scenario is about 3−4 TFSI oxygens, which may result from a monodentate or a bidentate coordination.[35]

Table 1 summarizes the fraction of lithium ions coordinating to one or two PEO chains (denoted as r_1 and r_2, respectively).

Table 1. Fraction of Lithium Ions Coordinating to One (r_1) or Two (r_2) PEO Chains, Mean Squared Chemical Bond Length b_0^2, Mean Squared End-to-End Vector $\langle R_e^2 \rangle$, and Mean Squared Radius of Gyration $\langle R_g^2 \rangle$ of the PEO Chains

system	r_1	r_2	b_0^2 [Å^2]	$\langle R_e^2 \rangle$ [Å^2]	$\langle R_g^2 \rangle$ [Å^2]
PEO	-	-	10.4	1904 ± 43	306 ± 35
$P_{20}S$	0.47	0.53	9.7	1573 ± 112	260 ± 42
			$P_{20}S\cdot x$ IL		
$P_{20}S\cdot0.66$ IL	0.53	0.47	9.7	1654 ± 121	272 ± 38
$P_{20}S\cdot3.24$ IL	0.76	0.24	9.6	1498 ± 57	249 ± 37
			$P_{20-\alpha x}S\cdot x$ IL		
$P_{16}S\cdot0.556$ IL	0.55	0.45	9.5	1767 ± 271	267 ± 50
$P_{12}S\cdot1.111$ IL	0.64	0.35	9.3	1349 ± 150	227 ± 43
$P_8S\cdot1.667$ IL	0.84	0.14	9.1	1840 ± 430	280 ± 80

Coordinations to three PEO chains were rarely observed and had a very brief lifetime of a few picoseconds only. Therefore, these events were neglected for the subsequent analysis. For the pure polymer electrolyte, the fractions of complexes involving one and two chains are nearly equal. Similar binding energies for both coordination types have also been found in quantum chemistry calculations.[34] The fraction of lithium ions coordinating to one PEO molecule increases with the IL content for both types of electrolytes.

In the case of $P_{20}S\cdot x$ IL, this is a consequence of the reduced PEO concentration, as it becomes less likely that a lithium ion encounters a second chain in the semidilute case. This is also confirmed by the observation that the fraction of Li^+ coordinating to one PEO chain increases linearly with x,

showing that the changes in the coordination sphere are purely statistical.

For $P_{20-\alpha x}S\cdot x$ IL, however, these trends are stronger than linear, which can be attributed to the fact that the PEO chains are successively removed from the system, and the remaining PEO chains become more crowded by Li^+ (see below). Thus, the different coordination shell can not solely be explained as a simple dilution effect.

3.2. Statical Polymer Structure. Due to the helical coordination structure of the PEO backbone, the local polymer structure changes, and the conformational phase space of the chain is reduced. Moreover, in the case of the ternary electrolytes, the additional IL molecules dilute the PEO chains, thus inducing a crossover from a polymer melt to a semidilute solution, which may also alter the equilibrium conformation of the polymer chains.[36] Table 1 summarizes the mean squared distance b_0^2 between two chemical monomers and the mean squared end-to-end vector $\langle R_e^2 \rangle$. Due to the crown-ether-like coordination of the PEO backbone, b_0^2 is smaller in all lithium-containing systems. For $P_{20-\alpha x}S\cdot x$ IL, this trend becomes more pronounced with increasing IL concentration.

A contraction of the polymer chain can also be observed for $P_{20}S\cdot x$ IL from $\langle R_e^2 \rangle$, which also decreases, whereas for $P_{20-\alpha x}S\cdot x$ IL no clear predictions can be made within the statistical uncertainties. When determining the ratio of $\langle R_e^2 \rangle$ and the radius of gyration $\langle R_g^2 \rangle$ (Table 1), one finds values close to the ideal ratio of six for a Gaussian chain[28] for all electrolytes, again indicating that on a global scale the chains are approximately Gaussian.

Also for the scaling of the Rouse mode amplitudes $\langle X_p^2 \rangle$, we observe only slight deviations from the respective curve for pure PEO (Figure 4). Here, the modes X_p were determined
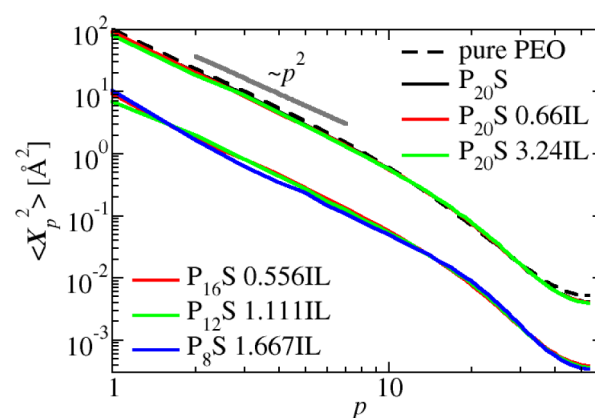

Figure 4. Rouse mode amplitudes $\langle X_p^2 \rangle$ in dependence of the mode number p calculated from the expression of the discrete Rouse model, i.e., $X_p(t) = (1/N)\sum_{n=1}^{N} \cos(p\pi(n-1/2)/N)R_n(t)$. The curves of the $P_{20-\alpha x}S\cdot x$ IL electrolytes have been shifted by 1 order of magnitude.

from the simulation data using the respective expression of the discrete Rouse model,[37] i.e., $X_p(t) = (1/N)\sum_{n=1}^{N} \cos(p\pi(n-1/2)/N)R_n(t)$, where the R_n denote the position vectors of the individual monomers. In the limit of low mode numbers p, we find the expected Rousean scaling $\langle X_p^2 \rangle \propto p^{-2}$, again demonstrating that the chain structure remains relatively ideal upon the addition of IL. Thus, no significant swelling of the chains can be observed, and the structural properties are similar as in neat PEO. On a local scale, however, the PEO chains

become rather contracted due to the helical coordination sphere of the lithium ions.

4. LITHIUM DYNAMICS

The MSDs of the lithium ions in the individual electrolytes are shown in Figure 5. For $P_{20}S \cdot x$ IL, one indeed observes an
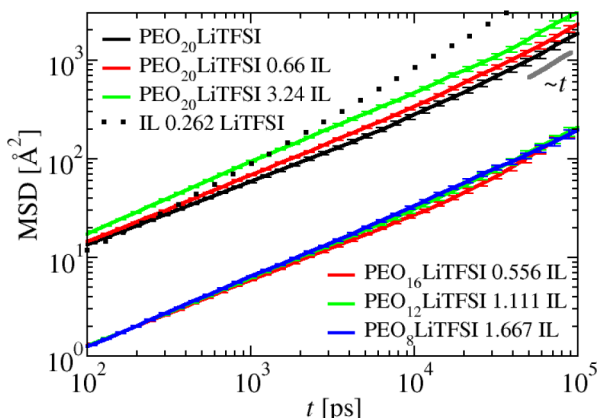

Figure 5. MSDs of the lithium ions in the individual electrolytes. The curves of the $P_{20-\alpha x}S \cdot x$ IL electrolytes have been shifted by 1 order of magnitude. The curve for the pure IL−salt solution $PYR_{13}TFSI \cdot 0.262$ LiTFSI is also shown for comparison.

increase of the lithium mobility upon the addition of IL. In particular, this increase becomes visible at 1−10 ns, whereas the onset to diffusive behavior occurs on the same time scale for all systems. Nevertheless, the MSDs are much smaller than for pure $PYR_{13}TFSI \cdot 0.262$ LiTFSI and the crossover to diffusion occurs much later. This is consistent with the observation that nearly all cations coordinate to the PEO chains, and that the lithium transport in the ternary electrolytes changes not too drastically as compared to $P_{20}S$. Interestingly, for $P_{20-\alpha x}S \cdot x$ IL, no significant difference in the lithium MSD can be found.

In the following, we will employ the lithium ion transport model to rationalize these observations. First, we will focus on the intersegmental transfer and the diffusion along the chain, followed by an in-detail analysis of the polymer dynamics. Once all ingredients are combined, we will use the transport model to compute the macroscopic lithium diffusion coefficients from the numerical data and compare these values to the experimental data from Passerini et al.[12]

4.1. Lithium Ion Transfer Mechanism. First, we will study the lithium ion transfer between two different polymer chains, which is vital for the long-range cation transport and thus any macroscopically measurable lithium diffusion. That is, when only considering the diffusion along the chain and the PEO dynamics as possible transport mechanisms, the ion remains confined to a finite volume characterized by the radius of gyration of the PEO chains. Moreover, the diffusion of the center of mass of the polymer chain becomes irrelevant in the experimentally relevant long-chain limit. Previous MD simulations focusing on this mechanism have shown that the dynamics of the lithium ion is independent from its past after such transfer processes,[20] leading to Markovian behavior for time scales larger than τ_3, and that these processes can thus be regarded as renewal events in the spirit of the DBP model.[22]

We start with the investigation of the detailed mechanism of the cation transfer process. During most transfers, the ion is coordinated to two PEO chains simultaneously (i.e., the leaving

chain and the entering chain) as a transition state. In some events, the cation is also temporarily coordinated by TFSI anions only and migrates to another PEO chain in this way, which will be discussed below.

Figure 6 shows a histogram of the lifetimes τ of the intermediate in which a Li^+ is coordinated by two PEO chains
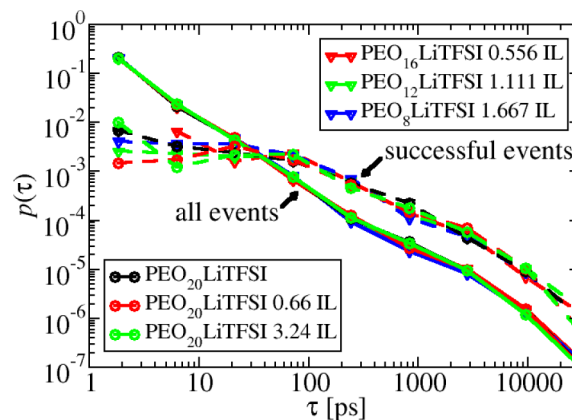

Figure 6. Histogram of the lifetimes τ of the intermediate complexes involving two PEO chains which facilitate the cationic transfer. Solid, all events; dashed, successful events only (see text).

(solid lines). One clearly observes that the resulting distribution is very broad. Whereas most complexes exist only briefly (i.e., a few picoseconds), some exist over nearly the whole simulation length of 200 ns. For all electrolytes, no significant difference can be found for $p(\tau)$, suggesting a rather universal mechanism. This is also reasonable when keeping in mind that the lithium coordination sphere containing two PEO chains is relatively compact and that the surrounding molecules thus hardly affect the transfer process once the complex has formed.

Of course, it is questionable if also the brief coordinations in Figure 6 can result in a successful cation transfer since the separation of the leaving chain and the simultaneous formation of a new, stable coordination sphere on the entering chain will need a certain time. For this purpose, Figure 6 also shows $p(\tau)$ for complexes which resulted in a successful transfer. The criterion for a successful transfer was that the lithium ion remained detached from the old chain for at least 100 ps, which was motivated by a more detailed analysis revealing that non-Markovian, short-time backjumps to the old chain occur up to about 100 ps (not shown). From Figure 6 one indeed observes that the probability for short τ is lower for real renewal events (dashed lines). Again, the curves are nearly identical for all electrolytes.

To study the transfer mechanism in more detail, we monitored the progress of the cation transfer as follows: When a second PEO chain enters the coordination sphere of a cation that is already coordinated to a PEO molecule, the EO coordination number n at the first chain naturally decreases. For brief coordinations of the second chain, the crown-ether-like structure of the first chain will hardly be perturbed. On the other hand, for longer times, one would expect a rather symmetric coordination by both PEO chains, leading to smaller n. In the case of a successful cation transfer, the EO coordination number decreases even further to zero. The minimum coordination number n_{min} that is reached during τ can therefore be used to monitor the progress and the success of the cation transfer.

Figure 7 shows the probability $p(n_{min})$ to find a specific minimum coordination number n_{min} as well as the probability
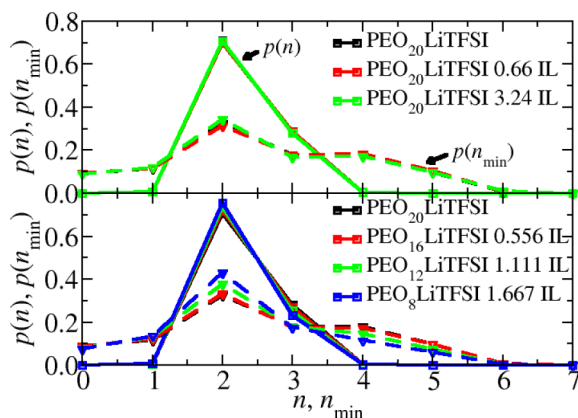

Figure 7. Probability $p(n)$ to find a specific EO coordination number n for a cation coordinated to two PEO chains (solid) as well as the probability $p(n_{min})$ to find a minimum EO coordination number n_{min} on the first PEO chain during the lifetime of the complex (dashed).

to find any coordination number n on the first PEO chain during τ. For $p(n)$, one clearly observes that on average 2–3 EOs of each chain coordinate to the Li$^+$ (solid lines). This coordination is independent from the IL concentration as expected from the dense packing of the coordination sphere. In the case of $p(n_{min})$, significant probabilities are found for $n_{min} = 0$, $n_{min} = 3 − 5$, and, most pronounced, $n_{min} = 2$. These values correspond to the following situations: a complete transfer, in which the first chain no longer coordinates to the ion (leading to $n_{min} = 0$), a brief coordination by the second chain, in which the first chain is still tightly bound with $n_{min} = 3−5$ EOs, and a symmetric coordination of both chains ($n_{min} = 2$). When increasing the IL concentration, one notices that the brief coordinations corresponding to $n_{min} = 4−5$ become less likely for P$_{20−\alpha x}$S·x IL. As a consequence, the relative probability that a complex with $n_{min} = 2$ is formed increases. For P$_{20}$S·x IL, no such effect can be observed, and $p(n_{min})$ remains basically unaltered by the presence of the IL. This indicates that the increased probability of $n_{min} = 2$ for P$_{20−\alpha x}$S·x IL is not related to a simple concentration effect, which would also be present for P$_{20}$S·x IL but rather to the fact that the PEO molecules are successively substituted by IL. Due to this substitution, each PEO chain coordinates to more cations, resulting in an enhanced rigidity of the PEO backbone, which impedes the formation of the helical structure with $n = 4−5$ and thus leads to a larger value for $p(n_{min} = 2)$.

In total, a complete cation transfer with $n_{min} = 0$ has the same relative probability of about 10% for all IL concentrations and EO:Li ratios. Obviously, the critical step is the encounter of a second PEO chain or, more precisely, a free PEO segment. Once the complex has formed, it decays according to a universal distribution of lifetimes (Figure 6). A remarkable feature, however, is the fact that although $p(n_{min} = 2)$ (which corresponds to a symmetric coordination by both PEO chains) for P$_{20−\alpha x}$S·x IL increases with x the complete transfer with $p(n_{min} = 0)$ does not become more likely, indicating that other, less trivial factors affect the outcome of a PEO−Li$^+$−PEO encounter.

It is also worth noting that, in contrast to earlier findings from MD simulations of a PEO/LiBF$_4$ electrolyte,[20] no significant influence of the anion on the PEO-to-PEO transfer could be observed. Most likely, the minor importance of the TFSI anions for the transfer arises from the suppressed tendency to form ion pairs or higher-order ionic clusters as compared to BF$_4^−$.

4.2. Renewal Time. To determine τ_3, we counted the number of transfer processes N_{trans} from the simulations. As above, brief transfers and successive backjumps after less than 100 ps were excluded, while on the other hand transfer processes via the anions were also counted since they serve as a renewal process in the same way. Subsequently, the τ_3 values were determined according to $\tau_3 = t_{max} N_{Li+}/N_{trans}$, where $t_{max} = 200$ ns is the simulation length and $N_{Li+} = 27$ is the number of lithium ions in the simulation box.

The individual values for τ_3 are summarized in Table 2. One observes for both the P$_{20}$S·x IL and the P$_{20−\alpha x}$S·x IL electrolytes that τ_3 increases with increasing IL concentration. Since the PEO molecules become more and more diluted, this can at least partly be explained as a concentration effect. However, the stronger increase for P$_{20−\alpha x}$S·x IL indicates that not only the reduced PEO concentration but also the reduced number of free EOs, which are necessary for a successful transfer, lead to an increase of τ_3. To understand these trends in more detail, we will figure out the individual contributions to the τ_3 values in the following. When the lithium ion moves through the electrolyte, it has to encounter a free PEO segment to be transferred (naturally, above the glass-transition temperature, the segments themselves also show significant motion). The probability for such an event can be estimated on the basis of a few structural parameters: First, the volume element into which the Li$^+$ moves has to be occupied by PEO. Here, the probability to encounter any PEO segment (free or bound) can be obtained from the volume fraction of PEO in the simulation cell, i.e., V_{PEO}/V. Second, the PEO segment has to be free,

Table 2. Average Residence Times τ_3 of a Lithium Ion at a Given PEO Chain^a

system	τ_3 [ns]	V_{PEO}/V	p_{EO}^{free} [%]	p_{IL} [%]	$p_{trans,IL}$ [%]	$\langle\tau_{Li}\rangle_{IL}$ [ns]	$\langle\Delta R_{Li}^2\rangle_{IL}$ [Å^2]
P$_{20}$S	17.1 ± 1.3	0.87	72.3	0.02	2.5	0.25 ± 0.08	31 ± 8
			P$_{20}$S·x IL				
P$_{20}$S·0.66 IL	18.4 ± 1.4	0.72	71.9	0.03	1.0	0.58 ± 0.31	34 ± 13
P$_{20}$S·3.24 IL	24.1 ± 1.3	0.43	73.1	0.36	8.5	0.99 ± 0.22	102 ± 26
			P$_{20−\alpha x}$S·x IL				
P$_{16}$S·0.556 IL	25.0 ± 2.0	0.70	65.2	0.07	4.6	0.38 ± 0.14	34 ± 10
P$_{12}$S·1.111 IL	28.4 ± 2.2	0.52	54.7	0.43	13.7	0.88 ± 0.20	79 ± 17
P$_8$S·1.667 IL	32.7 ± 2.5	0.35	36.7	2.50	38.2	2.10 ± 0.31	226 ± 51

^{a}Here, $p_{trans,IL}$ is the probability that the lithium ion is transferred by TFSI anions; $\langle\tau_{Li}\rangle_{IL}$ corresponds to the average duration the Li$^+$ is coordinated to TFSI only in such a transfer; and $\langle\Delta R_{Li}^2\rangle_{IL}$ is the average squared distance the ion covers during this time.

which is necessary to form the helical coordination sphere. Here, we defined a free segment as a block of at least four free EOs, which occurs with probability p_{EO}^{free}. The overall probability to encounter a free PEO segment (at least four EOs) is then given by the product of V_{PEO}/V and p_{EO}^{free} (both quantities are shown in Table 2). Apart from these structural ingredients, one also needs dynamical information on how fast the PEO segments (and the attached lithium ions) move. That is, the faster both the lithium ions and the PEO segments rearrange, the more opportunities the ions have to find a free PEO segment and to be transferred. Although the effect of the IL on the polymer dynamics will be discussed in Section 5, we nevertheless use the parameter C_R (Table 3), which is the

Table 3. Parameters Characterizing the Two Intramolecular Transport Mechanisms (See Text for Further Explanation)[a]

system	τ_1 [ns]	$\langle \mathbf{R}_e^2 \rangle_{eff}$ [Å^2]	τ_R [ns]	τ_2 [ns]	C_R [Å^2 ns$^{-1/2}$]	C_2 [Å^2 ns$^{-1/2}$]
PEO	-	1979	22	-	151.5	-
P$_{20}$S	147	1662	45	167	89.0	46.2
P$_{20}$S·x IL						
P$_{20}$S·0.66 IL	140	1570	37	89	92.7	59.8
P$_{20}$S·3.24 IL	127	1571	24	68	115.2	68.4
P$_{20-\alpha x}$S·x IL						
P$_{16}$S·0.556 IL	181	1479	43	145	81.0	44.1
P$_{12}$S·1.111 IL	208	1359	35	145	82.5	40.5
P$_8$S·1.667 IL	301	1151	28	104	78.1	40.5

[a]The values for pure PEO are also shown for comparison.

prefactor of the Rouse-like MSD$\propto t^{1/2}$ for the average EOs, as an anticipatory measure for the polymer dynamics. Since C_R quantifies the motion of the average EOs, it implicitly contains the dynamics of both the free PEO segments and the lithium ions (due to the cooperative motion with the bound EOs, which are also contained in C_R; see below). When plotting the product $(V_{PEO}/V)p_{EO}^{free}C_R$ versus the observed τ_3, we find a nearly perfect linear relationship (correlation coefficient −0.99) within the statistical error of τ_3. This demonstrates that τ_3 is essentially determined by three factors: the volume fraction of PEO and the fraction of free PEO segments (or, alternatively, the volume concentration of free PEO segments), on one hand, and the polymer dynamics on the other hand.

Table 2 also shows the probability $p_{trans,IL}$ that a TFSI-supported transfer takes place ($p_{trans,IL} = N_{trans,IL}/N_{trans}$; i.e., the number of transfers in which the Li$^+$ is intermediately coordinated to TFSI only relative to the total number of transfers). For high IL concentrations, it becomes more likely for a lithium ion to migrate through the IL-rich regions of the electrolyte. Since this scenario is less likely for P$_{20}$S·x IL, one can conclude that the transfer via TFSI in P$_{20-\alpha x}$S·x IL is mainly caused by the crowded PEO chains and the lower fraction of free EOs. Also shown in Table 2 is the mean time $\langle \tau_{Li} \rangle_{IL}$ the Li$^+$ is coordinated to TFSI only in a PEO−TFSI−PEO transfer and the average squared distance $\langle \Delta \mathbf{R}_{Li}^2 \rangle_{IL}$ the lithium ion covers during this period. The values for $\langle \tau_{Li} \rangle_{IL}$ and $\langle \Delta \mathbf{R}_{Li}^2 \rangle_{IL}$ show trends similar to $p_{trans,IL}$: With increasing IL fraction and decreasing number of free EOs (P$_{20-\alpha x}$S·x IL electrolytes), both $\langle \tau_{Li} \rangle_{IL}$ and $\langle \Delta \mathbf{R}_{Li}^2 \rangle_{IL}$ show a significant increase. From the Einstein relation $D_{Li,IL} = \langle \Delta \mathbf{R}_{Li}^2 \rangle_{IL}/(6\langle \tau_{Li} \rangle_{IL})$, we find values close to the lithium diffusion coefficient in PYR$_{13}$TFSI·0.262 LiTFSI ($D_{Li,IL} = 14.014$ Å^2 ns^{-1}). Thus, for P$_{20-\alpha x}$S·x IL, a change of the entire lithium transport mechanism becomes

visible, and the PEO−TFSI−PEO transitions may substantially contribute to the overall lithium MSD for sufficiently large values of $p_{trans,IL}$ and $\langle \Delta \mathbf{R}_{Li}^2 \rangle_{IL}$. However, it will turn out later that the impact of the IL-mediated transport is negligible for most investigated electrolytes (see discussion in Section 6).

4.3. Diffusion along the Chain. To quantify the quasi-one-dimensional random walk of the lithium ions along the PEO chains, all EOs have been numbered consecutively, and the mean squared change $\langle \Delta n^2(t) \rangle$ of the average EO index n has been computed (Figure 8).
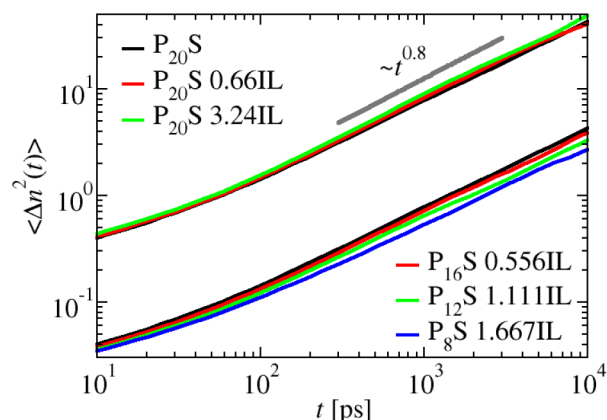
Figure 8. Mean square change of the average EO index $\langle \Delta n^2(t) \rangle$ for the P$_{20}$S·x IL and P$_{20-\alpha x}$S·x IL electrolytes. The curves of the P$_{20-\alpha x}$S·x IL electrolytes have been shifted by 1 order of magnitude.

Starting from about 100 ps, the dynamics crosses over to a regime that is only slightly subdiffusive (i.e., $\langle \Delta n^2(t) \rangle \propto t^{0.8}$). Qualitatively, this behavior is found for all compositions. For P$_{20}$S·x IL, no significant change of $\langle \Delta n^2(t) \rangle$ can be observed when varying the IL concentration, indicating that the motion along the chain is basically determined by the characteristic motion of the PEO backbone and that the surrounding molecules (i.e., PEO chains or IL molecules) have virtually no influence on this mechanism. Interestingly, the magnitude of $\langle \Delta n^2(t) \rangle$ is essentially the same for lithium ions bound to one or to two PEO chains (not shown).

Switching to P$_{20-\alpha x}$S·x IL, one observes that the motion along the chain becomes slower with increasing IL concentration, especially for P$_{12}$S·1.111 IL and P$_8$S·1.667 IL (Figure 8), which can be attributed to the lower fraction of free EOs in the system. Interestingly, the value for the exponent of $\langle \Delta n^2(t) \rangle$ remains basically the same in this case, and only the magnitude of the functional form $\langle \Delta n^2(t) \rangle \propto t^{0.8}$ becomes slightly lower.

In principle, this type of motion could be quantified by the respective diffusion coefficient D_1 extracted from Figure 8 according to the Einstein relation

$$D_1 = \lim_{t \to \infty} \frac{\langle \Delta n^2(t) \rangle}{2t} \qquad (1)$$

Unfortunately, the $\langle \Delta n^2(t) \rangle$ curves in Figure 8 are not purely diffusive, whereas on larger time scales the statistics are too bad, since the ions are additionally transferred between distinct PEO chains, thus making it impossible to track the motion along the chain any further. To estimate the net effect of this mechanism, i.e., the number of traversed monomers during τ_3, D_1 was approximately estimated as

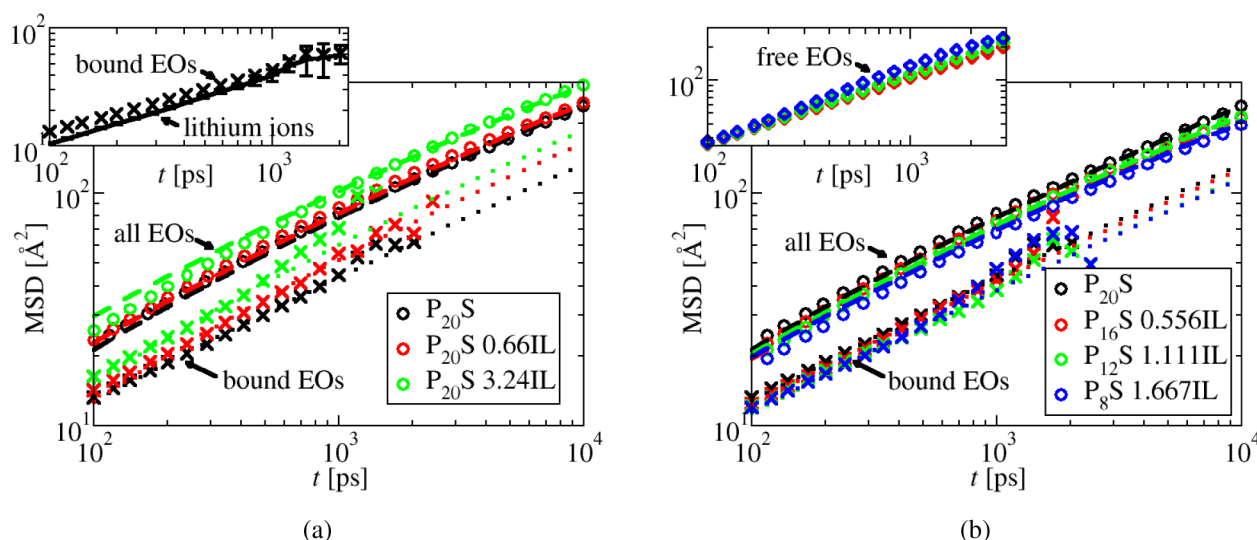(a)   (b)

Figure 9. MSDs of the average EOs (circles), bound EOs (crosses), lithium ions bound to these EOs ($|\Delta n(t)| \leq 1$, solid lines in the inset of (a)). The inset of (b) shows the MSD of the central EOs of a PEO segment consisting of at least seven free EOs. All MSDs have been computed in the center-of-mass frame of the PEO chain. The dashed and the dotted lines show the respective Rouse fits.

$$D_1(\tau_3) = \frac{\langle \Delta n^2(\tau_3) \rangle}{2\tau_3} \qquad (2)$$

Since the maximum observation time in Figure 8 is lower than the τ_3 values, we assumed that the scaling $\langle \Delta n^2(t) \rangle \propto t^{0.8}$ persists until $t = \tau_3$ and simply extrapolated the curves in Figure 8. Subsequently, the time scale τ_1 was calculated by the respective expression from the transport model[20]

$$\tau_1 = \frac{(N-1)^2}{\pi^2 D_1} \qquad (3)$$

Table 3 summarizes the resulting τ_1 values. For the $P_{20-\alpha x}S \cdot x$ IL electrolytes, one clearly observes an increase of τ_1 with increasing IL concentration since more and more EOs become involved in complexes with lithium and the PEO backbone becomes less mobile. Contrarily, for the $P_{20}S \cdot x$ IL electrolytes, τ_1 decreases only slightly, which can mainly be attributed to the dependence of τ_1 on τ_3 (eq 2). In total, the motion along the chain basically remains unaltered in these electrolytes, as also suggested by Figure 8.

5. POLYMER DYNAMICS

5.1. Segmental Dynamics. To quantify the segmental polymer motion, the MSDs $\langle \Delta \mathbf{R}^2(t) \rangle$ of the EOs relative to the center of mass of the PEO chain have been calculated (Figure 9). This quantity has been computed for all EOs (i.e., irrespective of the presence of an ion), for EOs bound to a lithium ion and for the respective attached ions. The criterion to consider a cation or EO as bound was that the average EO index of the ion did not change more than one, i.e., $|\Delta n(t)| \leq 1$, for all time frames during t. For the bound EOs, no further distinction between additional coordinations of the lithium ion to, e.g., another PEO chain or a TFSI molecule was made. Thus, these effects are already implicitly contained in the curves in Figure 9. Of course, one might wonder if cations bound to two PEO molecules show the same dynamical characteristics as ions bound to a single polymer chain, as the $Li(PEO)_2$ complexes could be viewed as temporary cross-links. A more detailed analysis (published in the SI of our previous study)[17]

indeed revealed that there is a conceptual difference between these two coordinations. However, the temporary cross-links do not affect the polymer dynamics but rather the motion along the chain: whereas lithium ions coordinated to one chain are transported by both intramolecular mechanisms, ions bound to two chains experience the polymer dynamics only. This is due to the fact that the PEO chains move reptation-like along their own contour past the cation, which results in a nonzero $\langle \Delta n^2(t) \rangle$ (Figure 8) but does not contribute to the overall lithium transport. Since there is no qualitative effect of the coordination on the polymer dynamics (possibly also due to the fact that the exchange between both coordination types is sufficiently fast), we proceed to characterize the average dynamics of the bound PEO segments with a single τ_2 only.

The average EOs (circles) show typical Rouse-like motion with the characteristic relaxation time τ_R. The dynamics of the bound EOs (crosses) is qualitatively the same but protracted. Therefore, it is possible to characterize the intramolecular dynamics of the bound EOs by using a larger, effective Rouse time τ_2. The lithium ions attached to these EOs (inset, solid lines) closely follow the bound EOs, which gives evidence for their cooperative motion. On short time scales, the MSD of the EOs is larger than the lithium MSD due to the additional internal degrees of freedom of the PEO backbone, but the MSD of the bound cations catches up on longer time scales (approximately 1 ns). Due to the collective motion, τ_2 also characterizes the dynamics of the attached lithium ions.

Figure 9 also shows the Rouse fits

$$\langle \Delta \mathbf{R}^2(t) \rangle = \frac{2 \langle \mathbf{R}_e^2 \rangle}{\pi^2} \sum_{p=1}^{\infty} \frac{\left[1 - \exp\left(-\frac{tp^2}{\tau_R} \right) \right]}{p^2} \qquad (4)$$

for the average (dashed lines) and the bound EOs (dotted lines). It is important to mention that the precise value of τ_2 obtained from these fits also depends on the value of $\langle \mathbf{R}_e^2 \rangle$ entering the prefactor of eq 4. To obtain a fit consistent with the plateau value at large t, the MSDs of the average EOs were fitted using two parameters, i.e., τ_R and $\langle \mathbf{R}_e^2 \rangle_{\text{eff}}$. In this way, the $\langle \mathbf{R}_e^2 \rangle$ values in eq 1 are replaced by an effective mean squared

1120

dx.doi.org/10.1021/jp409800r | J. Phys. Chem. B 2014, 118, 1113−1125

end-to-end vector $\langle \mathbf{R}_e^2 \rangle_{\text{eff}}$, characterizing the maximum accessible intramolecular distance for the cations. Once $\langle \mathbf{R}_e^2 \rangle_{\text{eff}}$ was determined from the MSDs of the average EOs, the MSDs of the bound EOs were fitted using this value in combination with a single fit parameter τ_2 only. The fitting parameters $\langle \mathbf{R}_e^2 \rangle_{\text{eff}}$, τ_R, and τ_2 are summarized in Table 3 (deviations from our previous study[38] on $P_{20}S$ arise from the shorter simulation length of about 27 ns and the slightly modified fitting procedure).

In the case of $P_{20}S \cdot x$ IL, $\langle \mathbf{R}_e^2 \rangle_{\text{eff}}$ decreases only slightly when IL is added. The $\langle \mathbf{R}_e^2 \rangle_{\text{eff}}$ values are in reasonable agreement with the respective $\langle \mathbf{R}_e^2 \rangle$ values in Table 1. Compared to pure PEO, the $\langle \mathbf{R}_e^2 \rangle_{\text{eff}}$ values are about 16–20% lower in these systems and show good agreement with the respective values in Table 1. This demonstrates that the PEO chains in these electrolytes behave relatively ideally, thus additionally validating our analysis in terms of the Rouse model. Both τ_R and τ_2 decrease significantly, clearly indicating that the dynamics of the PEO segments becomes faster with increasing IL concentration. Therefore, the IL can be regarded as a plasticizer. Due to the enhanced polymer mobility, the lithium ions also move faster while they are coordinated to a specific chain, and the overall lithium MSD increases as observed in Figure 5. A similar observation has been made experimentally for other plasticizers like ethylene/propylene carbonate[7,8] or short PEO chains embedded in a high molecular weight matrix.[6,8] Naturally, this effect has also been observed for ILs in the experiments[12] that motivated the present work.

For $P_{20-\alpha x}S \cdot x$ IL, $\langle \mathbf{R}_e^2 \rangle_{\text{eff}}$ clearly decreases when the PEO chains are successively substituted by IL molecules. The mismatch with the $\langle \mathbf{R}_e^2 \rangle$ values in Table 1 results from the different averaging procedure: whereas $\langle \mathbf{R}_e^2 \rangle$ is determined by the outer monomers only and thus rather characterizes the global polymer structure, $\langle \mathbf{R}_e^2 \rangle_{\text{eff}}$ contains contributions from all monomers, making it more susceptible to structural features on short and intermediate length scales. Note that the latter quantity is also statistically much better defined since the average is taken over all EOs instead of the outermost EOs only. The decrease of $\langle \mathbf{R}_e^2 \rangle_{\text{eff}}$ can be rationalized by the fact that more and more lithium ions coordinate to a specific PEO chain, thus diminishing the *average* intramolecular distances and, consequently, the maximum accessible displacement for most ions. At the same time, it is still possible that the PEO chains are stretched on a global scale, which might arise from, e.g., the electrostatic repulsion between distinct ions at a given chain (although for $P_{20-\alpha x}S \cdot x$ IL one cannot make clear predictions within the uncertainties of $\langle \mathbf{R}_e^2 \rangle$ in Table 1). In combination with the decline of $\langle \mathbf{R}_e^2 \rangle_{\text{eff}}$, the values for τ_R and τ_2 also decrease when the IL concentration is raised (Table 3). However, it must be pointed out that the τ_R and the τ_2 values of different electrolytes can only be quantitatively compared in conjunction with the precise value of $\langle \mathbf{R}_e^2 \rangle_{\text{eff}}$. Therefore, a direct comparison of τ_R and τ_2 is only valid for similar $\langle \mathbf{R}_e^2 \rangle_{\text{eff}}$, as in the case of $P_{20}S \cdot x$ IL . This is also highlighted by the observations from 5.1, where the EOs (both types) rather become slower with the IL fraction.

It is convenient to express $\langle \mathbf{R}_e^2 \rangle_{\text{eff}}$ and τ_R (or τ_2) within a single meaningful number. To this purpose, the prefactor of the characteristic Rouse-like motion for intermediate time scales (i.e., $\tau_R/N^2 \ll t \ll \tau_R$), $\langle \Delta \mathbf{R}^2(t) \rangle = (2\langle \mathbf{R}_e^2 \rangle/\pi^{3/2})(t/\tau_R)^{1/2}$, can be calculated, making it possible to directly measure the magnitude of the MSDs. Table 3 displays the constants $C_R = 2\langle \mathbf{R}_e^2 \rangle_{\text{eff}}/(\pi^3 \tau_R)^{1/2}$ and $C_2 = 2\langle \mathbf{R}_e^2 \rangle_{\text{eff}}/(\pi^3 \tau_2)^{1/2}$ for the individual

systems, thereby quantifying the mobilities of the average and the bound EOs, respectively. Here, one indeed observes the same trends as from the direct comparison of the MSDs: For $P_{20}S \cdot x$ IL, the segmental mobility expressed by C_R and C_2 clearly increases with the IL concentration, whereas it slightly decreases in the case of the $P_{20-\alpha x}S \cdot x$ IL electrolytes, meaning that also the lithium dynamics decreases. This behavior can again be explained by the reduced flexibility of the PEO backbone since the fraction of bound EOs increases when the PEO chains are gradually substituted by IL. Nevertheless, the plasticizing is also present for $P_{20-\alpha x}S \cdot x$ IL. This can be seen from the inset of Figure 9(b), which shows the MSDs of the central EOs of all those PEO segments consisting of at least seven free EOs. Again, one observes an increase in the polymer dynamics with increasing IL fraction. However, since the fraction of free EOs and the probability to encounter an entirely free PEO segment (cf. $p_{\text{EO}}^{\text{free}}$ in Table 2) are significantly lower, the plasticizing is barely visible in $P_{20-\alpha x}S \cdot x$ IL. Rather, for the average EOs, the progressive coordination of lithium ions to the PEO chains screens the plasticizing effect of the IL.

Finally, it is worth mentioning that for both investigated types of electrolytes the center-of-mass dynamics of the PEO chains becomes faster with increasing IL concentration. (The impact of this increase on the lithium diffusion coefficient will be discussed in Section 6). However, this observation can be easily rationalized by the fact that the motion of the individual chains is less hindered by other chains when the PEO concentration is reduced.

5.2. Hydrodynamic Interactions. An especially interesting effect of the IL on the polymer dynamics can be observed from the scaling of the Rouse-mode relaxation times. The correlators $\langle \mathbf{X}_p(0)\mathbf{X}_p(t) \rangle$ display a stretched exponential relaxation (not shown), and a Kohlrausch–Williams–Watts fit, $\langle \mathbf{X}_p(0)\mathbf{X}_p(t) \rangle / \langle \mathbf{X}_p^2 \rangle = \exp(-(t/\hat{\tau}_p)^\beta)$, was used to extract the parameters $\hat{\tau}_p$ and β (here, the hats have been used to avoid confusion with the time scales τ_1, τ_2, and τ_3 of the lithium ion transport model). The mean relaxation time $\langle \hat{\tau}_p \rangle$ is then given by $\langle \hat{\tau}_p \rangle = \hat{\tau}_p \beta^{-1} \Gamma(\beta^{-1})$, where Γ is the gamma function. The resulting scaling of $\langle \hat{\tau}_p \rangle$ is shown in Figure 10. Deviations from the values for $\tau_R \equiv \langle \hat{\tau}_1 \rangle$ in Table 3 result from the fact that the segmental MSD reflects an average over all modes, whereas $\langle \hat{\tau}_1 \rangle$ is determined from the first mode only.

For low mode numbers, both pure PEO as well as $P_{20}S$ exhibit the same scaling of approximately $\langle \hat{\tau}_p \rangle \propto p^{-2}$, thereby
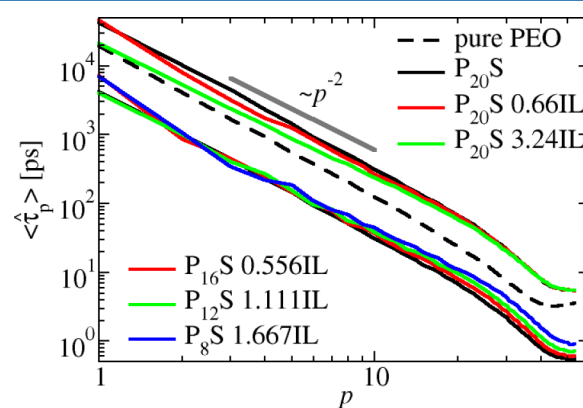

Figure 10. Average Rouse-mode relaxation times $\langle \hat{\tau}_p \rangle$ in dependence of the mode number p. The curves of the $P_{20-\alpha x}S \cdot x$ IL electrolytes have been shifted by 1 order of magnitude.

indicating that the global modes are Rousean. The absolute values of the $\langle \hat{\tau}_p \rangle$ are systematically higher for P$_{20}$S due to the decelerating effect of the lithium ions.

In contrast to this, one observes a clear decrease of the relaxation times at low p for P$_{20}$S·3.24 IL as compared to P$_{20}$S. As already observed from the fits of the segmental MSDs (Figure 9), P$_{20}$S·3.24 IL approximately has the same value for τ_R as pure PEO, whereas the local $\langle \hat{\tau}_p \rangle$ ($p \gg 1$) are basically the same as for the binary P$_{20}$S. However, a faster global relaxation combined with a similar local relaxation can only be realized by a less steep dependence of $\langle \hat{\tau}_p \rangle$ on p. These observations are compatible with a scenario in which hydrodynamic interactions, arising from the presence of the IL, contribute to the overall polymer motion. From an analytical point of view, these interactions can readily be taken into account via the Zimm model.[36,39] In its simplest form, i.e., when no swelling of the chains is present (cf. $\langle \mathbf{R}_e^2 \rangle$ in Figure 1 and $\langle \mathbf{X}_p^2 \rangle$ in Figure 4), the equilibrium distribution of the chain conformation is Gaussian as in the Rouse model. Therefore, the static polymer properties remain unaffected, and only the dynamics is altered, leading to a scaling of the relaxation times of $\hat{\tau}_p \propto p^{-3/2}$.

Interestingly, for P$_{20-ax}$S·x IL, the scaling of the $\langle \hat{\tau}_p \rangle$ for intermediate p does not change significantly. However, the uncertainties of these curves increase when the PEO chains are successively replaced by IL (up to 60% in the worst case, i.e., $p = 1$ for P$_8$S·1.667 IL). For the local modes, the $\langle \hat{\tau}_p \rangle$ increase with the IL concentration, again highlighting the reduced flexibility of the PEO backbone. Therefore, in total, the replacement of PEO by IL rather leads to a decrease of the polymer dynamics, and the plasticizing effect of the IL is not sufficient to compensate for the slowing down of the PEO segments caused by the attached lithium ions.

Although the scaling of the $\langle \hat{\tau}_p \rangle$ is rather Zimm-like[39] (i.e., $\langle \hat{\tau} \rangle_p \propto p^{-3/2}$) for P$_{20}$S·$x$ IL, especially for P$_{20}$S·3.24 IL, the segmental MSD nevertheless shows the characteristic Rousean proportionality MSD $\propto t^{1/2}$ for $t \geq 1$ ns (Figure 9) instead of the respective Zimm scaling[36] MSD $\propto t^{2/3}$. Only on time scales up to about 1 ns, the MSD of the average EOs is lower and slightly steeper than the Rouse predictions for P$_{20}$S·3.24 IL. This is in clear contrast to P$_{20}$S, for which the PEO curve is larger than the Rouse prediction due to the additional internal degrees of freedom of the PEO backbone. Thus, this feature reflects another minor imprint of the hydrodynamic interactions. On larger length scales, however, the hydrodynamic interactions are screened since the monomer concentration in the PEO–IL solutions is still relatively high. Consequently, the chains interpenetrate strongly as in the pure polymer melt, and the momentum transfer via the low-molecular solvent acts only on short length scales. A similar dynamical behavior has also been reported previously for semidilute solutions of model polymers[40] simulated by a combination of stochastic Langevin dynamics and Lattice Boltzmann techniques.[41] Since the motion on larger scales is still Rousean, we also left eq 4 unchanged to extract τ_2 for the P$_{20}$S·x IL electrolytes.

When discussing the effect of the hydrodynamic interactions on the Rouse modes, it should be mentioned that for a simulation system with periodic boundary conditions finite size effects will always be present. This artifact arises due to the circumstance that a given PEO monomer interacts not only with its image in the neighbor cell but also with all other monomers of the replicated polymer chain. However, this finite-size effect has a different impact on the center-of-mass motion ($p = 0$) and the internal polymer dynamics. The leading-order finite-size correction to the Rouse modes for $p > 0$ is only proportional to L_{box}^{-3} (with L_{box} being the length of the simulation box) and is thus usually negligible, as has been demonstrated both analytically[42] and numerically.[43] Contrarily, the main correction to the center-of-mass diffusion is proportional to L_{box}^{-1}. In this case, the interaction between periodic images can be interpreted as an effective increase of the hydrodynamic radius of the polymer chain, which impedes its diffusion.[42] From simulation data of a related system,[44] we can estimate that in the present study the relative importance of the finite-size effect is roughly 15%. Since the diffusive regime of the center-of-mass motion of PEO is in any event subject to large uncertainties (relative error 10−25%) and its contribution to the lithium diffusion is irrelevant in the long-chain limit, we did not take this correction into account for our further analysis.

6. COMPARISON WITH EXPERIMENTS

Finally, we compare the predictions of the lithium transport model to the experimental data taken from ref 12. Of course, a direct comparison of D_{Li} as extracted from Figure 5 is impossible since the center-of-mass motion of the short PEO chains ($N = 54$) in our simulations significantly contributes to the lithium diffusion, whereas most experimental studies focus on the long-chain limit (e.g., $M_w = 4.000.000$ g/mol in ref 12). However, due the explicit N-dependence of the three time scales,[20] i.e., $\tau_1 \propto N^2$, $\tau_2 \propto N^2$, and $\tau_3 \propto N^0$, and using the fact that the center-of-mass motion vanishes for $N \to \infty$, this problem can be easily circumvented.

For the scaling of τ_2, entanglement effects may become relevant, which would manifest itself by a steeper dependence of the polymer relaxation time on N for chain lengths larger than the entanglement length N_e. However, if $\tau_3 < \tau_e$, meaning that the lithium ion leaves the chain before the latter begins to reptate, the dynamical contribution to the lithium ions is still Rousean.[36] In the case of PEO, experiments revealed that the entanglement regime sets in from about $N \approx 75$.[45,46] On the basis of these observations, one can estimate τ_e according to $\tau_e = \tau_R(N = 75) = \tau_R(75/54)^2$. For P$_{20}$S, this leads to $\tau_e \approx 87$ ns, which is substantially larger than τ_3. Also in the case of the highly plasticized P$_{20}$S·3.24 IL one finds $\tau_e \approx 46$ ns $> \tau_3$. Therefore, the lithium ion leaves the PEO chain before the tube constraints become noticeable, and the transport model can also be applied in the limit of long chains.

Due to the renewal events (i.e., the interchain transfer), D_{Li} can be expressed as

$$D_{Li}(N) = \frac{\langle g_{12}(N, \tau_3) \rangle_{M3}}{6\tau_3} + D_{PEO}(N) \tag{5}$$

where $\langle g_{12}(\tau_3) \rangle_{M3}$ corresponds to an averaged, elementary step length between two successive renewal events (abbreviated as M3) and is characterized by the intramolecular transport mechanisms (i.e., the diffusion along the chain and the polymer dynamics). The center-of-mass motion of the PEO chains with length N is characterized by the diffusion coefficient D_{PEO}. As shown in earlier work,[20] g_{12} can be described by a Rouse-like expression

$$g_{12}(t) = \frac{2\langle \mathbf{R}_e^2 \rangle}{\pi^2} \sum_{p=1}^{\infty} \frac{\left[1 - \exp\left(-\frac{tp^2}{\tau_{12}} \right) \right]}{p^2} \tag{6}$$

where $1/\tau_{12} = 1/\tau_1 + 1/\tau_2$ is a combined relaxation rate due to both mechanisms. As argued in Section 5, lithium ions coordinated to two PEO chains experience no effective transport due to the diffusion along the chain (see also SI of ref 17). However, with respect to eq 6, this effect can be easily captured. For a sufficiently fast exchange between coordinations to one and to two PEO chains, the average intramolecular lithium MSD $\overline{g}_{12}$ is simply determined by the structural quantities r_1 and r_2 (Table 1)

$$\overline{g}_{12}(t) = r_1 g_{12}(t) + r_2 g_2(t) \tag{7}$$

That is, for the fraction r_1 of cations bound to one PEO chain, eq 6 remains valid, whereas for ions bound to two chains with $\tau_{1,2PEO} \to \infty$, only τ_2 is important. In the case of exponentially distributed residence times at the distinct PEO chains (which is fulfilled to a good approximation in our simulations except for shortest residence times lower than 300 ps, which account only for a few percent), one can write down an analytical expression for the average MSD at a given chain

$$\langle g_{12}(\tau_3)\rangle_{M3} = \frac{1}{\tau_3}\int_0^\infty dt\, \exp\left(-\frac{t}{\tau_3}\right)g_{12}(t)$$

$$= \frac{2\langle \mathbf{R}_e^2\rangle}{\pi^2}\sum_{p=1}^\infty \frac{1}{p^2}\left[1 - \frac{1}{p^2\frac{\tau_3}{\tau_{12}}+1}\right] \tag{8}$$

Solving this expression numerically, values for D_{Li} were obtained for $N = 54$ (D_{Li}^{sim}) and $N \to \infty$ (D_{Li}^∞), which are summarized in Table 4 (here, a correction similar to eq 7 has

Table 4. Lithium Diffusion Coefficient D_{Li} Calculated by the Lithium Transport Model (In Particular Equations 5 and 8) for $N = 54$ (D_{Li}^{sim}) and $N \to \infty$ (D_{Li}^∞)[a]

system	D_{Li}^{sim} [Å² ns⁻¹]	D_{Li}^∞ [Å² ns⁻¹]	D_{Li}^{exp} [Å² ns⁻¹] (ref 12)
$P_{20}S$	2.945 (2.947)	1.947 (1.949)	0.052 ($P_{20}S$)
		$P_{20}S{\cdot}x$ IL	
$P_{20}S{\cdot}0.66$ IL	3.542 (3.545)	2.309 (2.313)	0.118 ($P_{20}S{\cdot}2.0$ IL)
$P_{20}S{\cdot}3.24$ IL	4.257 (4.292)	2.392 (2.434)	0.126 ($P_{20}S{\cdot}4.0$ IL)
		$P_{20-\alpha x}S{\cdot}x$ IL	
$P_{16}S{\cdot}0.556$ IL	2.573 (2.581)	1.511 (1.520)	0.051 ($P_{10}S{\cdot}1.0$ IL)
$P_{12}S{\cdot}1.111$ IL	2.716 (2.765)	1.311 (1.366)	0.063 ($P_{10}S{\cdot}2.0$ IL)
$P_8S{\cdot}1.667$ IL	2.812 (3.092)	1.166 (1.487)	0.046 ($P_5S{\cdot}1.0$ IL)

[a]The values in parentheses for D_{Li}^{sim} and D_{Li}^∞ are corrected values, for which the lithium migration through IL-rich regions has been taken into account. Experimental values[12] for similar compositions at $T = 323$ K are also shown.

been applied). For the calculation of D_{Li}^{sim}, D_{PEO} was simply extracted from the simulation. When comparing D_{Li}^{sim} with the lithium diffusion coefficients directly extracted from Figure 5, we find reasonable agreement between both values (although the diffusion coefficients from the MSDs are about 5–20% higher, which is due to the fact that the lithium motion has not yet become fully diffusive and the statistical uncertainties are relatively large in the long-time regime). However, when using the transport model to calculate the lithium MSDs as in our previous work[17] (which was done by simulating a random-walk motion whose step length was given by eq 6 and in which random reorientations at given time steps sampled from a Poisson process modeled the renewal events), we find

quantitative agreement within the error bars for all systems, showing that the predictions of our model are consistent with the numerical data.

In the following, we will compare our results with the experimental data (D_{Li}^{exp}) at $T = 323$ K taken from ref 12. Despite the temperature gap between simulation and experiment, we observe identical trends: For a similar dilution series, in which the IL is *added* to $P_{20}S$, D_{Li}^{exp} also increases significantly with increasing IL content. In contrast to this, D_{Li}^{exp} rather decreases when the PEO chains are *substituted* by IL, and consequently, the EO:Li ratio decreases.

As already discussed in context with the segmental PEO motion (Section 5.1), these observations can be understood as follows: In the case of $P_{20}S{\cdot}x$ IL, the IL acts as a plasticizer, and the enhanced polymer dynamics leads to a faster lithium ion dynamics. On the other hand, when the EO:Li ratio simultaneously decreases as for $P_{20-\alpha x}S{\cdot}x$ IL, the remaining PEO chains become more and more rigid, which approximately cancels the plasticizing effect of the IL.

Thus, two opposing trends related to the segmental mobility can be found in ternary polymer electrolyte−ionic liquid mixtures: the slow down of the polymer motion with decreasing EO:Li ratio (also encountered in the binary systems) and the plasticizing due to the IL, leading to an enhancement of the polymer dynamics (i.e., both the segmental and the center-of-mass motion). Naturally, for the technologically relevant long-chain limit, the enhancement of the center-of-mass motion of the PEO chains is irrelevant. For these reasons, one should keep in mind that especially the polymer segments remain mobile enough when designing new electrolyte materials.

It should be pointed out that the D_{Li} values in Table 4 do not contain the contribution from those lithium ions which are coordinated by IL molecules only and thus move faster. In particular, for the electrolytes $P_{12}S{\cdot}1.111$ IL and $P_8S{\cdot}1.667$ IL, for which this additional, fourth mechanism becomes relevant (Table 2), this would lead to noticeably higher D_{Li} values in Table 4. Here, a correction to D_{Li} can easily be estimated: At a given time, the fraction of lithium ions coordinated by TFSI only is given by p_{IL} (Table 2). Since we found that the dynamics of these ions is similar to that in $PYR_{13}TFSI{\cdot}0.262$ LiTFSI (see discussion in Section 4.2), one can use the respective lithium diffusion coefficient ($D_{Li,IL} = 14.014$ Å² ns⁻¹) to estimate their contribution to the overall diffusion coefficient, whereas the relative contribution of the remaining lithium ions (coordinated to PEO) is still described by eq 5

$$D_{Li}^{corr}(N) = (1 - p_{IL})D_{Li}(N) + p_{IL}D_{Li,IL} \tag{9}$$

The respective corrected values for D_{Li}^{sim} and D_{Li}^∞ are given in parentheses in Table 4. As already expected from the values of p_{IL}, significant contributions arise only for $P_{12}S{\cdot}1.111$ IL and $P_8S{\cdot}1.667$ IL ($p_{IL} = 0.4\%$ and 2.5%, respectively), whereas D_{Li} for all other electrolytes remains basically unaltered.

Thus, for most electrolytes, the value of D_{Li} is determined by essentially three contributions (eq 5): the intrachain distance $\langle g_{12}(\tau_3)\rangle_{M3}$ the ion covers while connected to the same chain, the center-of-mass motion of the PEO molecules characterized by D_{PEO}, and the renewal events measured by τ_3, which facilitate the diffusive motion of the ions in the long-time limit for $N \to \infty$. Moreover, these trends may also oppose each other as in the case of $P_{20}S{\cdot}x$ IL. For these reasons, it is desirable to quantify how far the modified intrachain transport

1123

dx.doi.org/10.1021/jp409800r | J. Phys. Chem. B 2014, 118, 1113−1125

and the altered renewal rates contribute to the overall change of D_{Li} relative to the pure polymer electrolyte $P_{20}S$.

Table 5 shows the percentage by which the intramolecular contributions ($\langle g_{12}(\tau_3)\rangle_{M3}$), the center-of-mass motion of the

Table 5. Percentage Changes of the Intramolecular Contribution $\langle g_{12}(\tau_3)\rangle_{M3}$, the Renewal Rates τ_3^{-1}, the Center-of-Mass Motion D_{PEO}, and the Resulting D_{Li} Value Relative to $P_{20}S$ for (a) $N = 54$ and (b) $N \to \infty$

system	$\langle g_{12}(\tau_3)\rangle_{M3}$	τ_3^{-1}	D_{PEO}	D_{Li}
(a) $N = 54$				
$P_{20}S$	±0	±0	±0	±0
$P_{20}S \cdot x$ IL				
$P_{20}S \cdot 0.66$ IL	+22	−7	+30	+20
$P_{20}S \cdot 3.24$ IL	+54	−29	+92	+45
$P_{20-\alpha x}S \cdot x$ IL				
$P_{16}S \cdot 0.556$ IL	+9	−32	+4	−13
$P_{12}S \cdot 1.111$ IL	+6	−40	+30	−8
$P_8S \cdot 1.667$ IL	+5	−48	+50	−5
(b) $N \to \infty$				
system	$\langle g_{12}(\tau_3)\rangle_{M3}$	τ_3^{-1}	D_{PEO}	D_{Li}
$P_{20}S$	±0	±0	-	±0
$P_{20}S \cdot x$ IL				
$P_{20}S \cdot 0.66$ IL	+28	−7	-	+19
$P_{20}S \cdot 3.24$ IL	+73	−29	-	+23
$P_{20-\alpha x}S \cdot x$ IL				
$P_{16}S \cdot 0.556$ IL	+14	−32	-	−22
$P_{12}S \cdot 1.111$ IL	+12	−40	-	−33
$P_8S \cdot 1.667$ IL	+15	−48	-	−40

PEO chains (D_{PEO}), and the renewal rates (τ_3^{-1}) as well as the overall D_{Li} values change relative to the pure polymer electrolyte $P_{20}S$ for $N = 54$ and $N \to \infty$.

For $P_{20}S \cdot x$ IL one clearly observes that the intramolecular contribution increases with the IL concentration, mainly as a result of the increased segmental mobility. For finite PEO chains, the enhanced D_{PEO} value additionally increases the lithium motion. In contrast to this, the contribution of the renewal processes decreases for these electrolytes. However, the plasticizing effect overcompensates this decrease, and D_{Li} increases for both $N = 54$ and $N \to \infty$.

Remarkably, the relative intramolecular contribution also increases for $P_{20-\alpha x}S \cdot x$ IL, although the enhancement is weaker than for $P_{20}S \cdot x$ IL. At first glance, this may contradict the findings presented in Section 5.1, where it was observed that both the diffusion along the PEO chain and the segmental motion become slower when IL is added to the system. However, this mismatch can easily be resolved by the following considerations: First, the fraction of lithium ions coordinating to one PEO chain only increases when going from $P_{20}S$ to $P_8S \cdot 1.667$ IL (Table 1). Since lithium ions coordinated to two polymer chains experience no effective transport via this mechanism (SI in ref 17), the diffusion along the PEO backbone becomes more efficient in this way. The second, more important effect leading to the observations from Table 5 is the fact that $\langle g_{12}(\tau_3)\rangle_{M3}$ is evaluated for different τ_3 (eq 8). Thus, with increasing τ_3 also the distance $\langle g_{12}(\tau_3)\rangle_{M3}$ increases, although this dependence is weaker than linear, and the overall D_{Li} diminishes in this case. Consistently, calculating the individual values for $\langle g_{12}(\tau_3)\rangle_{M3}$ with a constant value of $\tau_3 = 17.1$ ns as observed for $P_{20}S$ (Table 2), the intramolecular

contribution indeed decreases for $P_{20-\alpha x}S \cdot x$ IL. The only contribution which displays a clear increase is D_{PEO}. Thus, for $N = 54$, D_{Li} diminishes only slightly, whereas a significant decrease can be found in the case of $N \to \infty$.

So far, we focused only on the high-temperature limit which we can address in our simulations. Interestingly, the relative increase of D_{Li}^{exp} upon the addition of IL becomes much more pronounced in the low-temperature regime.[12] Although additional simulations at low temperature would be too costly, we are nevertheless able to make some statements about this regime. For example, in the case of the addition of IL, it was reported that the glass-transition temperature T_g significantly decreases (up to 35 K) with increasing IL concentration,[12] which is a first indication that also at ambient temperatures the enhanced polymer dynamics contributes to a larger D_{Li}. In contrast to this, the experimentally observed decrease of T_g is significantly weaker for lower EO:Li ratios[12] (which resembles the case of IL substitution). Simultaneously, D_{Li}^{exp} approximately remains constant at 323 K. A detailed analysis of the low-temperature regime is already underway.

7. CONCLUSION

In this work, we presented an exhaustive MD simulation study on ternary polymer electrolytes consisting of PEO/LiTFSI and the ionic liquid $PYR_{13}TFSI$. In total, we investigated two different concentration series, namely, (a) the *addition* of the ionic liquid to $PEO_{20}LiTFSI$ and (b) the *substitution* of the PEO chains in $PEO_{20}LiTFSI$ by the ionic liquid, subject to the constraint of a constant lithium volume concentration. The latter electrolytes not only reflected an interpolation between $PEO_{20}LiTFSI$ and $PYR_{13}TFSI \cdot 0.262$ LiTFSI, but also served as model systems for electrolytes with lower EO:Li ratios. In addition to the simulations, we also utilized a lithium ion transport model[20] to express the effect of the ionic liquid on the lithium diffusion via a few microscopic parameters. On the basis of the combined insights from the simulations and the transport model, we were able to formulate general statements about how far the lithium ion transport mechanism changes when the composition of the electrolyte is varied.

In the case of sufficiently high EO:Li ratios (in particular 20:1), we find that the lithium transport almost exclusively takes place at the PEO chains and that the transport mechanism therefore is qualitatively the same as in binary $PEO_{20}LiTFSI$. For lower ratios, however, more and more lithium ions coordinate to a specific PEO chain, with the result that a progressive coordination by TFSI anions (both partially and totally) becomes visible. Accordingly, a completely new, fourth transport mechanism, in which the lithium ions are decoupled from the PEO chains, emerges due to the lack of free ether oxygens capable of binding the lithium ions. This mechanism may significantly contribute to the macroscopic lithium diffusion or even dominate it. From a theoretical perspective, we incorporated this mechanism into our transport model. For all electrolytes, we find reasonable agreement of the model predictions with the experimentally observed diffusion coefficients.[12]

Apart from these qualitative differences, the lithium transport is also altered on a quantitative level. For instance, the renewal rate τ_3^{-1}, characterizing the transfer between distinct PEO chains, decreases with increasing ionic liquid concentration and with decreasing fraction of free ether oxygens. Consequently, τ_3 is especially large for diluted electrolytes with crowded PEO chains (i.e., the $PEO_{20-\alpha x}LiTFSI \cdot x \, PYR_{13}TFSI$ systems).

Concerning the polymer dynamics, it turned out that the increase of the lithium diffusivity in $PEO_{20}LiTFSI \cdot x\ PYR_{13}TFSI$ can be attributed to the enhanced segmental mobility of the PEO chains and that the ionic liquid thus serves as a plasticizer. As a result of the faster PEO motion, also the lithium ions coordinating to the PEO chains become faster. Interestingly, the plasticization is also visible in the scaling of the Rouse-mode relaxation times, which exhibit a slightly Zimm-like scaling characteristic for semidilute polymer solutions. An opposing effect on the PEO dynamics, however, is the coordination to the lithium ions, which becomes especially pronounced for low EO:Li ratios. Accordingly, the average PEO dynamics in $PEO_{20-\alpha x}LiTFSI \cdot x\ PYR_{13}TFSI$ is slowed down by the progressive coordination of lithium ions, and the plasticizing effect of the ionic liquid becomes visible only for larger, entirely uncoordinated polymer segments. In summary, one therefore faces the situation that the segmental mobility of the PEO chains plays a decisive role in ternary polymer electrolytes: Whereas the lithium ions slow down the PEO chains, the ionic liquid accelerates the polymer motion. Thus, for the design of new battery materials, one should attempt to render the latter effect the dominating one.

■ ASSOCIATED CONTENT

Ⓢ Supporting Information

Simulation box sizes, radial distribution functions, and details of the lithium coordination shell as well as validation and benchmark of the AMBER code[23] employing the force field from refs 24 , 25, and 26. This material is available free of charge via the Internet at http://pubs.acs.org.

■ AUTHOR INFORMATION

Corresponding Author
*E-mail: diddo.diddens@ics-cnrs.unistra.fr.

Present Address
[†]Institut Charles Sadron, Université de Strasbourg, 23 Rue du Loess, BP 84047, 67034 Strasbourg, France (D.D.).

Notes
The authors declare no competing financial interest.

■ ACKNOWLEDGMENTS

■ REFERENCES

(1) Fenton, D. E.; Parker, J. M.; Wright, P. V. *Polymer* **1973**, *14*, 589.
(2) Armand, M. B. *Annu. Rev. Mater. Sci.* **1986**, *16*, 245−261.
(3) Gray, F. M. *Solid Polymer Electrolytes*; Wiley-VCH: New York, 1991.
(4) Bruce, P. G.; Vincent, C. A. *J. Chem. Soc., Faraday Trans.* **1993**, *89*, 3187−3203.
(5) Gang, W.; Roos, J.; Brinkmann, D.; Capuano, F.; Croce, F.; Scrosati, B. *Solid State Ionics* **1992**, *53*, 1102−1105.
(6) Borghini, M. C.; Mastragostino, M.; Zanelli, A. *Electrochim. Acta* **1996**, *41*, 2369−2373.
(7) Bandara, L. R. A. K.; Dissanayake, M. A. K. L.; Mellander, B. E. *Electrochim. Acta* **1998**, *43*, 1447−1451.
(8) Kim, Y. T.; Smotkin, E. S. *Solid State Ionics* **2002**, *149*, 29−37.
(9) Shin, J. H.; Henderson, W. A.; Passerini, S. *Electrochem. Commun.* **2003**, *5*, 1016−1020.
(10) Shin, J. H.; Henderson, W. A.; Appetecchi, G. B.; Alessandrini, E.; Passerini, S. *Electrochim. Acta* **2005**, *50*, 3859−3865.
(11) Shin, J. H.; Henderson, W. A.; Scaccia, S.; Prosini, P. P.; Passerini, S. *J. Power Sources* **2006**, *156*, 560−566.
(12) Joost, M.; Kunze, M.; Jeong, S.; Schönhoff, M.; Winter, M.; Passerini, S. *Electrochim. Acta* **2012**, *86*, 330−338.
(13) Adam, D. *Nature* **2000**, *407*, 938−940.
(14) MacFarlane, D. R.; Huang, J. H.; Forsyth, M. *Nature* **1999**, *402*, 792−794.
(15) MacFarlane, D. R.; Meakin, P.; Sun, J.; Amini, N.; Forsyth, M. *J. Phys. Chem. B* **1999**, *103*, 4164−4170.
(16) Zhou, Q.; Henderson, W. A.; Appetecchi, G. B.; Montanino, M.; Passerini, S. *J. Phys. Chem. B* **2008**, *112*, 13577−13580.
(17) Diddens, D.; Heuer, A. *ACS Macro Lett.* **2013**, *2*, 322−326.
(18) Nicotera, I.; Oliviero, C.; Henderson, W.; Appetecchi, G.; Passerini, S. *J. Phys. Chem. B* **2005**, *109*, 22814−22819.
(19) Kunze, M.; Paillard, E.; Jeong, S.; Appetecchi, G. B.; Schoenhoff, M.; Winter, M.; Passerini, S. *J. Phys. Chem. C* **2011**, *115*, 19431−19436.
(20) Maitra, A.; Heuer, A. *Phys. Rev. Lett.* **2007**, *98*, 227802.
(21) Rouse, P. E. *J. Chem. Phys.* **1953**, *21*, 1272−1280.
(22) Nitzan, A.; Ratner, M. A. *J. Phys. Chem.* **1994**, *98*, 1765−1775.
(23) Case, D. A. et al. *Amber 10*; University of California: San Francisco, 2008.
(24) Borodin, O.; Smith, G. D. *J. Phys. Chem. B* **2006**, *110*, 6279−6292.
(25) Borodin, O.; Smith, G. D. *J. Phys. Chem. B* **2006**, *110*, 6293−6299.
(26) Borodin, O.; Smith, G. D. *J. Phys. Chem. B* **2006**, *110*, 11481−11490.
(27) Toukmaji, A.; Sagui, C.; Board, J.; Darden, T. *J. Chem. Phys.* **2000**, *113*, 10913−10927.
(28) Berendsen, H. J. C.; Postma, J. P. M.; van Gunsteren, W. F.; DiNola, A.; Haak, J. R. *J. Chem. Phys.* **1984**, *81*, 3684−3690.
(29) Ryckaert, J. P.; Ciccotti, G.; Berendsen, H. J. C. *J. Comput. Phys.* **1977**, *23*, 327−341.
(30) van Belle, D.; Froeyen, M.; Lippens, G.; Wodak, S. J. *Mol. Phys.* **1992**, *77*, 239−255.
(31) Thole, B. T. *Chem. Phys.* **1981**, *59*, 341−350.
(32) Mao, G.; Saboungi, M.-L.; Price, D. L.; Armand, M. B.; Howells, W. S. *Phys. Rev. Lett.* **2000**, *84*, 5536−5539.
(33) Johansson, P.; Tegenfeld, J.; Lindgren, J. *Polymer* **1999**, *40*, 4399−4406.
(34) Baboul, A. G.; Redfern, P. C.; Sutjianto, A.; Curtiss, L. A. *J. Am. Chem. Soc.* **1999**, *121*, 7220−7227.
(35) Seo, D. M.; Borodin, O.; Han, S.-D.; Boyle, P. D.; Henderson, W. A. *J. Electrochem. Soc.* **2012**, *159*, A1489−A1500.
(36) Doi, M.; Edwards, S. F. *The Theory of Polymer Dynamics*; Oxford Science Publications: Clarendon, Oxford, 2003.
(37) Verdier, P. H. *J. Chem. Phys.* **1966**, *45*, 2118−2121.
(38) Diddens, D.; Heuer, A.; Borodin, O. *Macromolecules* **2010**, *43*, 2028−2036.
(39) Zimm, B. H. *J. Chem. Phys.* **1956**, *24*, 269−278.
(40) Ahlrichs, P.; Everaers, R.; Dünweg, B. *Phys. Rev. E* **2001**, *64*, 040501.
(41) Ahlrichs, P.; Dünweg, B. *J. Chem. Phys.* **1999**, *111*, 8225−8239.
(42) Dünweg, B.; Kremer, K. *J. Chem. Phys.* **1993**, *99*, 6983−6997.
(43) Pham, T. T.; Schiller, U. D.; Prakash, J. R.; Dünweg, B. *J. Chem. Phys.* **2009**, *131*, 164114.
(44) Chattoraj, J.; Heuer, A. *Private communication*, 2013, University of Münster, Germany.
(45) Appel, M.; Fleischer, G. *Macromolecules* **1993**, *26*, 5520−5525.
(46) Shi, J.; Vincent, C. A. *Solid State Ionics* **1993**, *60*, 11−17.